Talanta 84 (2011) 565–571

Contents lists available at ScienceDirect

Talanta

journal homepage: www.elsevier.com/locate/talanta

Fast DNA hybridization on a microfluidic mixing device based on pneumatic driving

Xin Wang [a], Xuemin Chen [a], Xiufeng Ma [b], Xiangwei Kong [b], Zhangrun Xu [a,*], Jianhua Wang [a,*]

[a] Research Center for Analytical Sciences, Northeastern University, Shenyang 110819, China
[b] Department of Mechanical Engineering and Automation, Northeastern University, Shenyang 110819, China

ARTICLE INFO

Article history:
Received 18 November 2010
Received in revised form 24 January 2011
Accepted 26 January 2011
Available online 2 February 2011

Keywords:
DNA hybridization
Microfluidics
Rapid mixing
Chaotic flow
Pneumatic pumping

ABSTRACT

A novel fluid mixing strategy was developed which significantly enhanced the efficiency of DNA hybridization. A pneumatic micro-mixing device consisting of two pneumatic chambers and an underneath DNA microarray chamber was built up. The fluid in the array chamber was pneumatically pumped alternately by the two pneumatic chambers. The chaotic oscillatory flow caused by the pumping greatly intensified the fluidic mixing. A homogeneous distribution of the tracer dye solution in the microarray chamber was observed after 2 s mixing with a pumping frequency of 24 Hz. Microarray DNA hybridization was substantially accelerated using this device, and the fluorescence intensity showed a plateau after oscillating 30 s at room temperature. The corresponding signal level of the dynamic hybridization was 12.5-fold higher than that of the static hybridization performed at 42 °C. A signal-to-noise ratio of 117 was achieved and the nonspecific adsorption of the targets to the sample array was minimized, which might be attributed to the strong shearing force generated during the pneumatic mixing process.

1. Introduction

Fast mixing and homogenization performance is of vital importance for most chemical reactions at microscale. In the microfluidic system, the flow is laminar in nature due to the small channel sizes. When no external energy or complex configuration is adopted, mixing is dominated merely by molecular diffusion which is extremely time-consuming. Generally, diffusion-based reaction such as DNA hybridization would become very inefficient when the mixing process is slower than the reaction itself. Since the mass transfer of the conventional static DNA hybridization is based on molecular diffusion, the target DNA has to travel slowly from the bulk solution to the sample surface. A rather long time was needed to accomplish the paring reaction to a sufficient extent, typically over 12 h. As DNA hybridization has been playing an important role in modern disease diagnosis, gene expression and genotyping, the low reaction efficiency became one of the urgent issues left to resolve [1–3].

Various attempts have been made to improve the hybridization kinetics along with signal uniformity by facilitating mass transfer. Some researchers developed electrokinetic methods which provided the means to dispense controlled samples directly to the hybridization arrays to accelerate the transportation of DNA molecules [4–6]. Cavitation microstreaming arising by ultrasonic power was used for DNA migration enhancement which resulted in up to 5-fold hybridization signal increment, and significantly improved the signal uniformity as compared to the results obtained in conventional diffusion-based biochips [7]. Fluid circulation and mixing in closed loop microfluidic devices were proved by the rotation of magnetic stirring bars. The reaction efficiency of microarray hybridization was enhanced 2–5-fold through fluid circulating and mixing with respect to diffusion-based static hybridization [8]. Another target solution recirculating method was achieved using a peristaltic pump, and the time of perfect match target–probe hybridization was shortened from 6 h to 2 h relative to static conditions [9]. Reciprocating flows were commonly generated by pushing target solution back and forth in microstructures, which improved hybridization performance in various degrees [10–14]. DNA hybridization was also carried out in a fluid mixer based on chaotic advection to deliver targets across a conventional glass slide array, and the hybridization signal intensities obtained were approximately 3–4-fold over a 24-h static hybridization [15]. Quake's group reported that chaotic mixing was generated by integrated peristaltic pumps and bridge channels with herring-bone protrusions fabricated in a microchip as well. This approach dramatically enhanced hybridization signals and improved sensitivity by nearly one order of magnitude relative to the conventional static hybridization method over the same length of time (2 h) [16]. It is obvious that most of these methods improved mixing efficiency by introducing moving elements or various other driving forces into

* Corresponding authors. Tel.: +86 24 83688944; fax: +86 24 83676698.
E-mail addresses: xuzr@mail.neu.edu.cn (Z. Xu), jianhuajrz@mail.neu.edu.cn (J. Wang).

0039-9140/$ – see front matter © 2011 Elsevier B.V. All rights reserved.
doi:10.1016/j.talanta.2011.01.065

the system. The hybridization efficiencies achieved through these approaches were favorable, but still worth striving for.

In the present work, we report the development of a micro-mixing device based on pneumatic pumping to generate chaotic oscillating flow for achieving efficient mixing. The alternate deformation of the pumping membranes results in strong convective flow in the reaction chamber. Numerical analyses were taken to simulate the flow pattern in the reaction chamber to further explain the mixing mechanisms. Fluidic experiments using a tracer were implemented to visualize and study the mixing performance. At last, fast polyacrylamide gel-based DNA microarray hybridization was achieved using the present mixing device.

2. Theory

Compared with static mixing based on molecular diffusion, active mixing based on strong chaotic convection is characterized by high efficiency [17–20]. Mixing based on chaotic convection is usually achieved by periodic perturbation of the flow fields [21]. In this manner, the contact areas of different fluidic elements were increased and the diffusion distance was shortened. As a result, the time of diffusion will be reduced according to Eq. (1). Finally, fluid mixing was accomplished by mass redistribution in the chamber where mass transfer and jumbling caused by the perturbation happened.

The physical process of mixing can be described using the convective–diffusion equation. Under the high Peclet number (P_e) condition, although the mass distribution alteration is generated by convection, mixing on the molecular level is still inevitably accomplished by molecular diffusion. Here, the convection item plays an important role in shortening diffusion distance and enlarging contact area, which can be described by the convective–diffusion Eq. (2). According to the classical fluid mechanics, the kinetics of fluid mobility can be described using N–S Eq. (3). Leaving body force out of consideration, pressure gradient and viscosity force become the dominate power sources of the velocity variation. Here, pressure gradient contributes to the convective acceleration which has the decisive effect towards mass space transmission. Consequently, good mixing performance is predictable when pressure gradient is formed in our micro-mixing chamber by introducing pressure difference between the fluid surfaces beneath the control chambers and at the fluid outlets during the pneumatic pumping process.

$$t \propto Dr^2 \tag{1}$$

$$\frac{\partial c}{\partial t} + (u \cdot \nabla)c = D\nabla^2 c \tag{2}$$

where D is the diffusion coefficient; r is the diffusion distance; t is the time; c is the concentration of the material; and u is the velocity vector.

$$u \cdot \nabla = u_x \frac{\partial}{\partial x} + u_y \frac{\partial}{\partial y} + u_z \frac{\partial}{\partial z}$$

$$\frac{\partial u}{\partial t} + (u \cdot \nabla)u = f - \frac{1}{\rho}\nabla p + \nu\nabla^2 u \tag{3}$$

$\partial u/\partial t$, local acceleration; $(u \cdot \nabla)u$, convective acceleration; f, field force, i.e., mass force; ν, kinematic viscosity, m^2 s, ρ, density; p, pressure.

3. Experimental

3.1. Fabrication of the pneumatic micro-mixing device

The pneumatic micro-mixing device consists of three layers. As illustrated in Fig. 1, a circular pneumatic chamber and an annular

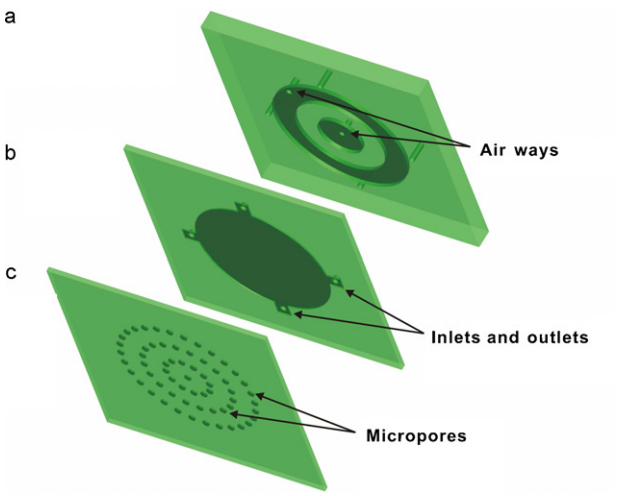

Fig. 1. The schematics of the three layers of the pneumatic micro-mixing device. (a) The first layer with pneumatic actuating chambers on the bottom; (b) the second layer with fluid chamber on the bottom; (c) the glass slide with micro-pore array on the upper side.

pneumatic chamber were designed on the bottom of the first PDMS layer (3 mm thick). The circular chamber is 3.0 mm in diameter and the homocentric annular chamber is a 1.5 mm wide circular loop with an outer diameter of 9.0 mm. Both of the pneumatic chambers are approximately 150 μm deep. A circular fluid chamber on the bottom of the second PDMS layer has four evenly distributed openings connected with capillaries (i.d. 530 μm). The fluid chamber is 300 μm deep and 9.0 mm in diameter. The PDMS actuating diaphragm on the top of the fluid chamber is approximately 100 μm thick. The third layer is a glass slide etched with micro-pores which construct an array of 39 spots. The micro-pores are about 150 μm deep and 0.8 mm in diameter. The dimension of the pneumatic mixing chip is 15 mm × 15 mm.

The mixing device was fabricated using a soft lithography technique resembling to the method described elsewhere [22]. The pattern of the channels was first printed onto a transparent film which is used as the photomask. The molds of the pneumatic chamber and the fluidic chamber were both fabricated with glass wet etching technique. The first layer with the pneumatic chambers was fabricated by pouring a mixture of PDMS (Sylgard 184, Dow Corning, Midland, Michigan, USA) into the glass positive mold. The second layer with the diaphragm and the fluid chamber was prepared by spin-coating PDMS mixture onto the glass positive mold. The third layer was made by etching the micro-pore array on a glass slide. After punching the access holes for the nitrogen introduction on each of the pneumatic chamber, the first layer was bonded onto the second layer following oxygen plasma treatment for 35 s in a plasma cleaner (PDC-32G-2 model, Harrick Scientific Corp., NY, USA), and then they were peeled off from the fluid chamber mold. The bonded two-layer structure was then sealed irreversibly onto the glass sheet following the punching of four access holes at each end of the openings. After that, the fused silica capillaries for fluid introduction and the homemade tie-ins for air way connection were fixed onto the mixing device. The micro-mixing chip was finally fitted into the pneumatic mixing system as illustrated in Fig. 2.

3.2. Fluidic mixing

The fluidic mixing efficiency was evaluated by introducing a 2-μL 8.0 μM Rhodamine 6G (Ubichem PLC, UK) into the center of the fluid chamber as a tracer and monitoring its distribution during the successive mixing cycles. After the deionized water was introduced into the fluid chamber, the tracer was injected into the

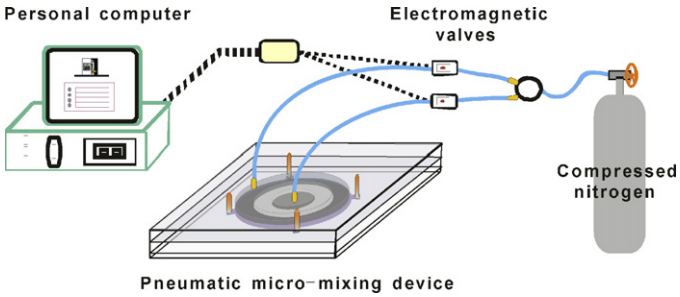

Fig. 2. Schematic diagram of the pneumatic micro-mixing system.

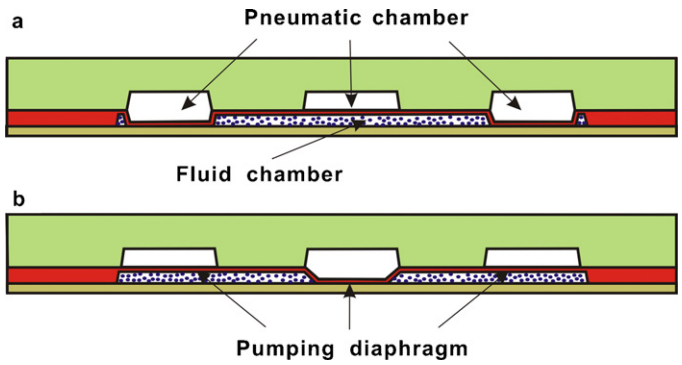

Fig. 3. The schematic illustration of the pneumatic fluidic mixing. The diaphragm deflected downwards when gas pressure was applied and resumed its shape quickly after the pressure was gone. (a) Pressure applied into the peripheral control chamber; (b) pressure applied into the central control chamber.

center of the fluid chamber using a syringe pump. And then, the syringe pump was removed from the micro-mixing device. The mixing procedure was conducted instantly by starting the control program. The diaphragm alternately agitated the fluid in the fluid chamber through its periodic deformation actuated by the nitrogen. A 40× microscope (ZTX3E, Ningbo Huaguang Precision Instrument Co., Ltd., China) and a digital camera (Power Shot A580, Canon INC., Japan) were used to record the mixing process. A visual communication suite (VCS-10132, Cole-Parmer, USA) was used for the quantitative analysis as a picture recording instrument. Mixing was assessed by computing the pixel intensity along the random axis of the fluid chamber using the Scion Image analysis software (Beta 4.0.2, Scion Corporation, USA).

3.3. Dynamic and static DNA hybridization

The hybridization of a 23-bp FITC labeled target was used to measure the average hybridization levels and local signal-to-noise ratios. Acrylamide-modified oligonucleotide and FITC-labeled oligonucleotide were synthesized by Takara (Takara Bio, Inc., Dalian, China). The sequences of the probe and the target are CGC AAT TCA TTG AGC GCA TTT AC with 5′ acrylamide, and GT AAA TGC GCT CAA TGA ATT GCG with 5′ FITC, respectively.

The glass slides for DNA immobilization (Yaohua glass instrument factory, Yancheng, China) were firstly steeped in 1 M NaOH for 2 h, then washed with deionized water to neutral, afterwards stored at 4 °C followed by Bind-Saline treatment. The preparation method of 3-D polyacrylamide gel-based DNA microarray was discussed in the work of Xiao et al. [23]. In the present work, 0.1 M sodium phosphate buffer (pH 7.5) was used as a substitute of water in the acrylamide-modified oligonucleotides solution. The 50 mL acrylamide-modified oligonucleotide solution contained 6% acrylamide monomer (29:1 acrylamide:bisacrylamide), 1% ammonium persulfate, 30% glycerol and 5 mL 10× TBE. The oligonucleotides solution was added to the micro-pores using a micropipette and the glass slide was then placed into a wet culture dish. After adding 30 μL TEMED, the dish was covered with a lid and left to stand at room temperature for 20 min. Thereafter, the gel array was washed using deionized water and stored at 4 °C. The hybridization buffer contained 0.9 M NaCl, 20 mM Tris–HCl (pH 8.0) and 40% methanamide, and the washing buffer contained 100 mM NaCl, 20 mM Tris–HCl (pH 8.0) and 40% methanamide [14]. FITC-labeled targets were diluted to a final concentration of 1 μM using the hybridization buffer. The glass slide immobilizing the gel array of DNA samples was sealed with the first two layers (the pneumatic control part) of the fluid micro-mixing chip, and then the tie-ins for air way connecting were fitted into the chip. After injecting 19 μL of the hybridization buffer into the fluid chamber, the two pneumatic pumps started working at 24 Hz, and the procedure lasted for 5–300 s. The dynamic DNA hybridizations were performed under room temperature (20–25 °C). When performing static hybridization, the target solution was manually added to the DNA probe spot array which was then placed onto a 42 °C heating device for 5–300 s. The chip was covered with wet culture dish while it was heated.

After hybridization, the glass slide was removed from the device, washed 10 times with 1 mL washing buffer to remove the unhybridized targets, dried and scanned using a microarray scanner (GeneTac LSIV scanner, Genomic Solutions, Cambridgeshire, UK) with an instrument setting of 50% PMT gain. The hybridization fluorescence intensities of both the dynamic and the static hybridization array were analyzed using Image-Pro Plus software (V 5.1, Media Cybernetics, USA).

4. Results and discussion

4.1. Chaotic oscillating mixing caused by pneumatic pumping

The characteristic features of PDMS, e.g., ease of molding, fabrication and bonding, transparency as well as flexibility make it a suitable material for pneumatically actuated valves/pumps in microfluidic systems [22,24]. When bearing air pressure, PDMS diaphragm presents elastic deformation and is thus capable of manipulating fluid conveniently given appropriate configuration in microfluidic systems. Continuous-flow polymerase chain reaction on microfluidic chip was achieved using this pneumatic pumping method [25]. In the present work, the two integrated pneumatic pumps worked alternatively to generate chaotic oscillating flow during the mixing process, and the working principle of which is illustrated in Fig. 3. When no gas pressure was applied in the central pneumatic chamber, the corresponding region in the fluid chamber kept open and allowed the fluid to stay therein, as shown in Fig. 3(a). In the meantime, the peripheral region of the fluid chamber kept closed owing to the gas pressure applied to the annular pneumatic chamber. As soon as the pressure was gone, the PDMS diaphragm resumes its shape thanks to its flexibility, which allowed the fluid to flow in. Simultaneously, the pressure applied in the central control chamber made the diaphragm deform downwards and extrude the underneath fluid away, as shown in Fig. 3(b). Identical operation went on until the mixing was finished. During the pneumatic pumping, the fluid surface pressures in the four capillaries were all 0 MPa. When the diaphragm was deforming and restoring, strong force was exerted on the underneath fluid and the contact area between the diaphragm and the fluid was bearing strong pressure. Therefore, pressure gradients were formed between the four outlets and the diaphragm contact area, which gave rise to convective acceleration that played the leading role in fast fluid mixing. Numerous vortexes in the fluid will then emerge at the boundaries of the diaphragms as a result of the velocity gradients invited by pressure gradients. As the vortex spread around, more fluid was

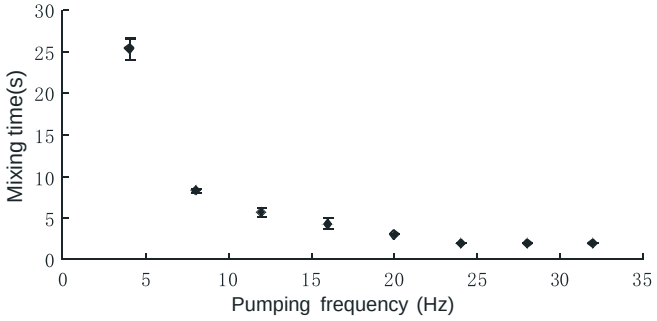

Fig. 4. Fluid mixing time with different pumping frequencies. The pumping diaphragm was 100 μm thick and a gas pressure of 0.08 MPa was used. The error bars were obtained from standard deviations ($n = 3$).

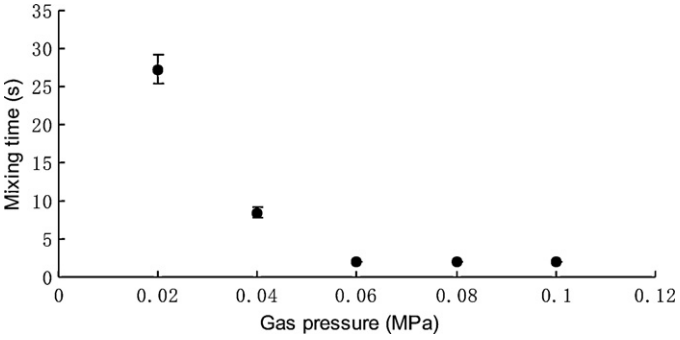

Fig. 5. The dependence of fluid mixing time on the gas pressure. The pumping diaphragm was 100 μm thick and a pumping frequency of 24 Hz was used. The error bars were obtained from standard deviations ($n = 3$).

brought into the vortex and strong convection was then achieved. When the PDMS diaphragms deformed alternately, they served as actuators which could achieve efficient mixing by continuous fluid oscillating that greatly increased the chaotic degree.

4.2. Effects of various factors on the mixing

A series of parameters, such as thickness of the diaphragm, pumping frequency and gas pressure, were studied for a better performance of the mixing device.

4.2.1. Thickness of the diaphragm

The PDMS membranes of various thicknesses could be readily obtained by spin-coating PDMS pre-polymer onto molds at different spinning velocities. PDMS as thin as possible would be preferable when used as pumping diaphragm, which allows larger deflection for fast opening and closing. In practice, diaphragms thinner than 100 μm tend to be damaged when peeled off from the molds. Therefore, a 100-μm thick diaphragm was chosen for this pneumatic mixing device, which concurrently maintained favorable deforming capacity, mechanical stability and ease of manufacturing.

4.2.2. Pumping frequency

In this work, the pumping frequency has great influence towards the mixing efficiency. As shown in Fig. 4, when the pumping frequency increased from 4 Hz to 24 Hz, the mixing time gradually shortened, and kept constant when the pumping frequency was higher than 24 Hz. The mixing time was obtained from the recorded time of the picture extracted from the fluid mixing video, and the mixing was evaluated by computing the pixel intensity along a random axis of the fluid chamber. A mixing time of 2 s was obtained at a pumping frequency of 24 Hz with a 100-μm thick diaphragm and a gas pressure of 0.08 MPa. When using the pumping frequency of 24 Hz for more than 3 min, tiny bubbles occasionally emerged in the fluid chamber. Fortunately these bubbles did not have much impact on the mixing in the present experiment.

4.2.3. Gas pressure

The effects of various gas pressures were also investigated at room temperature with a diaphragm of 100 μm and a pumping frequency of 24 Hz. The results were shown in Fig. 5. The mixing time was obtained in the same way as mentioned above. With an increase of the nitrogen pressure from 0.02 MPa to 0.06 MPa, a significant decrease of the mixing time was observed, which tend to be constant at a pressure of higher than 0.06 MPa. In practice, a 0.08 MPa nitrogen pressure was finally chosen to guarantee the mixing efficiency not to be affected by the minor variation of the thickness of the diaphragms caused by manual operation.

4.3. Numerical simulation

In order to investigate the mixing mechanism of this pneumatic micro-mixing device, FLUENT 5/6 was used for its computational fluidic dynamic analysis. As the fluid chamber can be seen as a flat circular column, a spacial axisymmetrical model representing the radial section was used to study the variation of the flow pattern. The perturbation caused by the gas pressure was defined as the movements of the chamber wall. Since the fluids at the chamber outlets were directly exposed to air, a 0 MPa condition at the outlets of the model was adopted. The K-e model of realizable was used to simulate the flow pattern, which gave rise to good results of the developments of the second flow (especially vertex flow) under low Reynolds number. Considering the configuration of the pneumatic pumping part of the fluid chamber, irregular flows were expected to appear at the margins of the diaphragms. To study the entire procedure of the perturbation, the movement of the chamber wall corresponded with the actual pneumatic pumping setting, and the computational domain was discretized with unstructured triangle grids. According to the simulation results shown in Fig. 6 (only half of the chamber intersection was shown), when the actuating diaphragm was deforming downwards, high fluid speed was generated at the margin of the diaphragm and plenty of vertexes were formed. The flow pattern in Fig. 6 only showed the original status of the vortex. With the increase of the valve actuation times, the small vortexes grow bigger and more circumjacent fluid was brought into the vortex, facilitating the mass transfer over the whole chamber. These results well explained the mechanism of the fast fluid mixing using the present pneumatic driving method.

4.4. Mixing evaluation and performance

In this work, the mixing was evaluated by computing the pixel intensity along the random axis of the fluid chamber using Scion Image analysis software. As shown in Fig. 7(a), when the tracer was initially injected into the center of the fluid chamber, there was a sharp gray level contrast between the central region and the surrounding area. After pneumatic mixing for 2 s with a pumping frequency of 24 Hz, the tracer distribution appeared to be homogeneous, as shown in Fig. 7(b). In another word, a complete mixing was achieved in 2 s for 19 μL fluid. Herein, the immethodical peaks in the curve were caused by the reflected light of the chamber edges (circled by broken line). Fig. 8 shows the mixing procedure of a dye solution at a pumping frequency of 24 Hz. Based on the results of numerical simulation and the fluid mixing analysis, we can draw the conclusion that fast mixing of massive fluid can readily be achieved in this micro-mixing device.

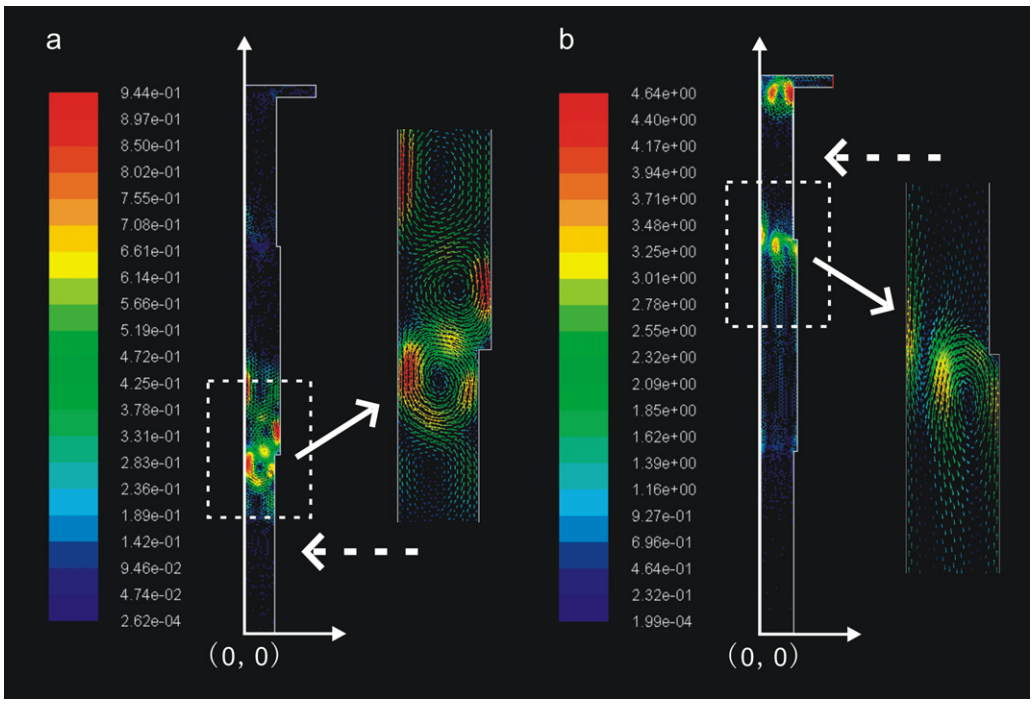

Fig. 6. The calculated velocity field in the pneumatic mixing device. (a) Vortexes generated when the central diaphragm was deforming downwards for the first time (a magnified image of the vortexes on the right side); (b) vortexes generated when the outer diaphragm was deforming downwards for the first time (a magnified image of the vortexes on the right side). The dotted arrows show the moving direction of the diaphragms. (0,0) indicates the center of the fluid chamber.

4.5. Fast DNA hybridization

A popular method was chosen for DNA immobilization on the glass slide: 3-D polyacrylamide gel-based DNA microarray using acrylamide-modified oligonucleotides which provides a high capacity for nucleic acid immobilization and a solution-mimicking environment for the hybridization [23,26]. Compared with DNA immobilization using NH_2-modified oligonucleotides, the present operation with acrylamide-modified oligonucleotide is much simple. However, to lower the background signal caused by the dry gel spots, electrophoresis was chosen for the post-hybridization treatment, which made the whole process less simplified. After dynamic hybridization using our mixing device, instead of electrophoresis treatment, the sample array was washed with washing buffer, and a 117-fold signal-to-noise ratio was obtained with no unfavorable strong background. The shear-stress exerted on hybridized target DNA during dynamic hybridization, which is adverse to nonspecific target bond, may explain the low background signal in our

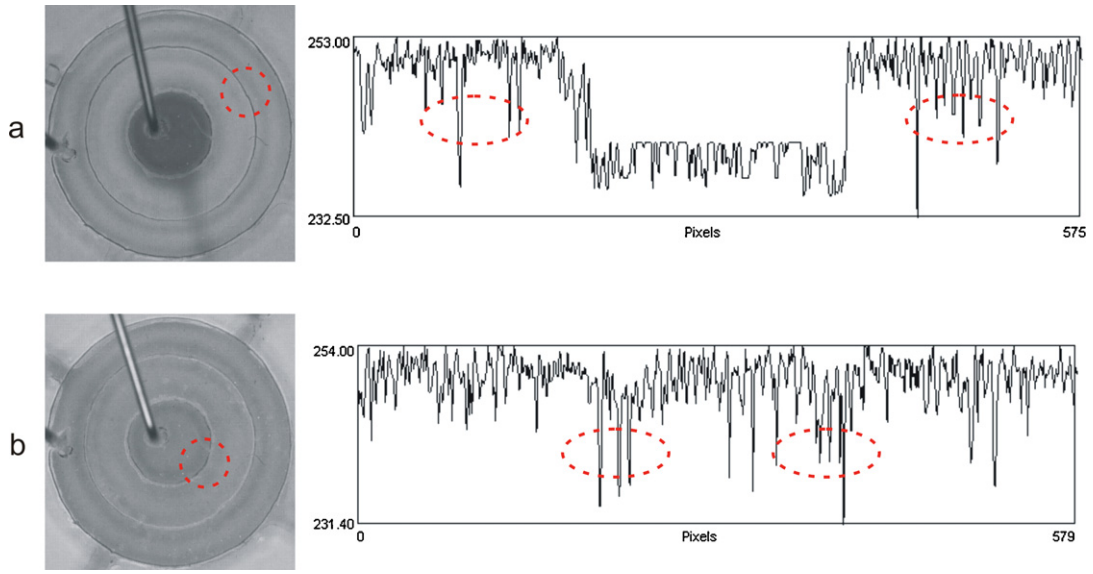

Fig. 7. The pixel intensity (gray value: 0–255) along the random axis of the fluid chamber before and after mixing. (a) The tracer was just injected into the mixing device; (b) complete mixing was achieved after 2 s pneumatic pumping. The immethodical gray values were caused by the borders of the pneumatic chambers (circled).

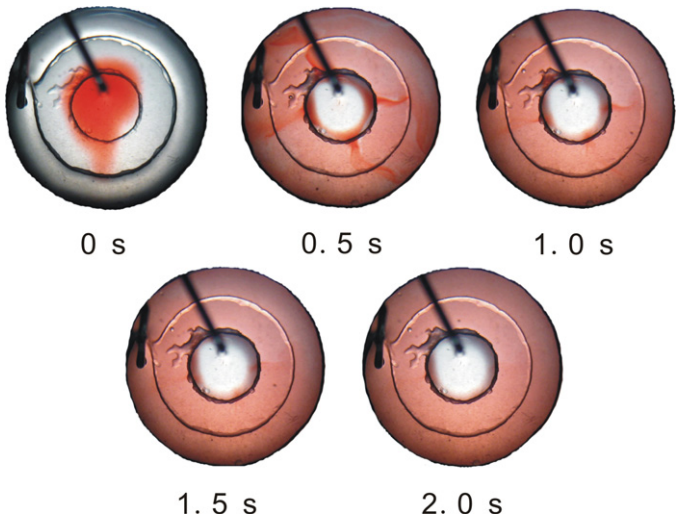

Fig. 8. Photographs of dye solution mixing in the 19-μL fluid chamber by using a 2-μL tracer.

pneumatic mixing dynamic hybridization system [15]. If the dry gel microarray was steeped in hybridization buffer for a while (e.g. 1 min) before injecting the target solution, the fluorescence background can be further decreased by over 2-fold.

We compared the hybridization signal intensity obtained in our pneumatic mixing dynamic hybridization device with signal intensity recorded in a conventional static hybridization system. Dynamic hybridization assay was performed in the PDMS pneumatic mixing device for 5–300 s with a pumping frequency of 24 Hz, while static hybridization was performed on a 42 °C heating device. Fig. 9, showed an obvious increase of the fluorescence intensity for the dynamic hybridization, which reached a plateau after 30 s. A 12.5-fold improvement of the signal intensity was achieved with respect to that by static hybridization at the same hybridization time. Although the fluorescence intensity of the static hybridization began to increase after 1 min, the signals of the static hybridization within 5 min were still very weak compared to that of the dynamic hybridization which was enhanced by effective agitation of the hybridization mixture. These results indicate that the efficiency of the DNA array hybridization was affected by the mass

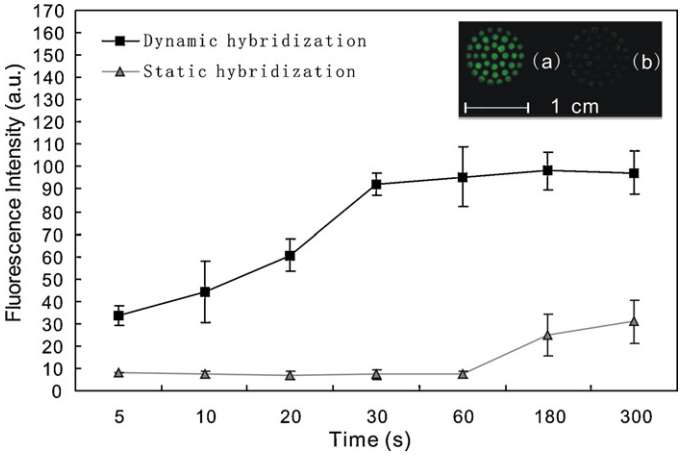

Fig. 9. The dependence of fluorescence intensity on the reaction time for both the dynamic and the static hybridization. Pneumatic pumping frequency, 24 Hz; target concentration, 1 μM. The fluorescence intensities were obtained by calculating the average values at 39 spots. The error bars were obtained from standard deviations (n = 3). The fluorescent scanning images of the 30 s dynamic hybridization (a) and static hybridization (b) were exhibited on the upper right corner.

transfer of the target solution. Chaotic oscillating flow caused by continual agitation greatly facilitated the target delivery from the bulk solution to the surface of the probe spots, and the opportunity for the targets to participate in hybridization reaction was remarkably enlarged. Hybridization was then accelerated owing to the fast supplement of the expended targets near the probe spots.

5. Conclusions

A novel micro-mixing device based on pneumatic driving was developed and the mixing capacity was studied by numerical simulation and fluid mixing with a tracer. Active mixing based on chaotic advection was achieved through periodic fluid oscillation generated by pneumatic pumping. It takes only 2 s to achieve a complete mixing. The mixing device is applied to the dynamic DNA hybridization, giving rise to a 12.5-fold improvement of the fluorescence signal intensity with respect to that by a conventional static DNA hybridization, and a 117-fold signal-to-noise ratio is obtained. Since the dynamic hybridization is taken at room temperature, better hybridization performance is predictable if a heating element is integrated into this device. In addition, high-throughput analysis can also be easily achieved by employing a microarrayer machine. It is noteworthy that the mixing performance of this device is independent of the electric property of the fluid. The approach is compatible with commercial high-density microarray slides, which will bring about high sensitivity and high throughput of DNA hybridization.

Acknowledgements

Financial support from Natural Science Foundation of China (20975019, 20805004, National Science fund for distinguished young scholars 20725517, and Major International Joint Research Project 20821120292), the 973 program (2007CB714503), the Program of New Century Excellent Talents in University (NCET-09-0274) and the Fundamental Research Funds for the Central Universities (N090105001, N100405003 and N100605002) are highly appreciated.

References

[1] V. Chan, D.J. Graves, S.E. McKenzie, Biophys. J. 69 (1995) 2243.
[2] M.R. Henry, P.W. Stevens, J. Sun, D.M. Kelso, Anal. Biochem. 276 (1999) 204.
[3] F.R.R. Teles, L.P. Fonseca, Talanta 77 (2008) 606.
[4] D. Erickson, X.Z. Liu, U. Krull, D.Q. Li, Anal. Chem. 76 (2004) 7269.
[5] C.F. Edman, D.E. Raymond, D.J. Wu, E.G. Tu, R.G. Sosnowski, W.F. Butler, M. Nerenberg, M.J. Heller, Nucleic Acids Res. 25 (1997) 4907.
[6] C. Gurtner, E. Tu, N. Jamshidi, R.W. Haigis, T.J. Onofrey, C.F. Edman, R. Sosnowski, B. Wallace, M.J. Heller, Electrophoresis 23 (2002) 1543.
[7] R.H. Liu, R. Lenigk, R.L. Druyor-Sanchez, J.N. Yang, P. Grodzinski, Anal. Chem. 75 (2003) 1911.
[8] P.K. Yuen, G.S. Li, Y.J. Bao, U.R. Muller, Lab Chip 3 (2003) 46.
[9] H.H. Lee, J. Smoot, Z. McMurray, D.A. Stahl, P. Yager, Lab Chip 6 (2006) 1163.
[10] C.W. Wei, J.Y. Cheng, C.T. Huang, M.H. Yen, T.H. Young, Nucleic Acids Res. 33 (2005) e78.
[11] Y.J. Liu, C.B. Rauch, Anal. Biochem. 317 (2003) 76.
[12] R. Lenigk, R.H. Liu, M. Athavale, Z.J. Chen, D. Ganser, J.N. Yang, C. Rauch, Y.J. Liu, B. Chan, H.N. Yu, M. Ray, R. Marrero, P. Grodzinski, Anal. Biochem. 311 (2002) 40.
[13] N.B. Adey, M. Lei, M.T. Howard, J.D. Jensen, D.A. Mayo, D.L. Butel, S.C. Coffin, T.C. Moyer, D.E. Slade, M.K. Spute, A.M. Hancock, G.T. Eisenhoffer, B.K. Dalley, M.R. McNeely, Anal. Chem. 74 (2002) 6413.
[14] C.Y. Li, X.L. Dong, J.H. Qin, B.C. Lin, Anal. Chim. Acta 640 (2009) 93.
[15] M.K. McQuain, K. Seale, J. Peek, T.S. Fisher, S. Levy, M.A. Stremler, F.R. Haselton, Anal. Biochem. 325 (2004) 215.
[16] J. Liu, B.A. Williams, R.M. Gwirtz, B.J. Wold, S. Quake, Angew. Chem. Int. Ed. 45 (2006) 3618.
[17] H. Aref, J. Fluid Mech. 143 (1984) 1.
[18] H. Aref, Phil. Trans. R. Lond. A 333 (1990) 273.
[19] J.M. Ottino, Sci. Am. 260 (1989) 54.
[20] J.M. Hertzsch, R. Sturman, S. Wiggins, Small 3 (2007) 202.
[21] K.S. Ryu, K. Shaikh, E. Goluch, Z.F. Fan, C. Liu, Lab Chip 4 (2004) 608.

[22] M.A. Unger, H.P. Chou, T. Thorsen, A. Scherer, S.R. Quake, Science 288 (2000) 113.
[23] P.F. Xiao, L. Cheng, Y. Wan, B.L. Sun, Z.Z. Chen, S.Y. Zhang, C.Z. Zhang, G.H. Zhou, Z.H. Lu, Electrophoresis 27 (2006) 3904.
[24] H. Becker, L.E. Locascio, Talanta 56 (2002) 267.
[25] Z.R. Xu, X. Wang, X.F. Fan, J.H. Wang, Microchim. Acta 168 (2010) 71.
[26] M.F. Kane, M. Loda, G.M. Gaida, J. Lipman, R. Mishra, H. Goldman, J.M. Jessup, R. Kolodner, Cancer Res. 57 (1997) 808.